Supercritical Phase Fischer-Tropsch Synthesis: Catalyst Pore-Size Effect

Li Fan, Kohshiroh Yokota, and Kaoru Fujimoto
Dept. of Synthetic Chemistry, Faculty of Engineering, The University of Tokyo, Tokyo 113, Japan

The Fischer-Tropsch synthesis reaction was conducted in a supercritical fluid medium using a fixed-bed reactor. Tailor-made catalyst supports which had sharp pore diameter distributions were prepared by the pH swing method. The relationships between the catalyst pore structure and the catalytic activity or the product distribution were studied. The influence of the catalyst pore size on the mass transfer of reactants and products was also characterized. The catalyst pore size affected not only catalytic activity but also product selectivity. The diffusion of reactants inside the catalyst pellets in the supercritical fluid media was simulated and the effects of catalyst pore size and catalyst particle size on catalytic performances were consistent with simulation results.

Introduction

As a new reaction phase brought into the classical Fischer-Tropsch (F-T) synthesis reaction process, the supercritical phase F-T reaction showed unique characteristics such as quick diffusion of reactant gas, effective removal of reaction heat, and *in situ* extraction of high molecular weight hydrocarbons (wax) (Yokota and Fujimoto, 1989-1991).

The F-T synthesis reaction, which has been commercially operated using the solid-catalyzed gas-phase reaction, was inevitably accompanied by the local superheating of the catalyst surface as well as the production of heavy wax. The local superheating of the catalyst may cause the deactivation of the catalyst and also an increase in the methane formation. Heavy wax, which does not vaporize under the reaction conditions, may plug the micropores of the catalyst and, in some cases, the catalyst bed itself.

The slurry-phase F-T reaction process, on the other hand, in which a slurry of the catalyst particles in mineral oil is used as a reaction medium, has been developed to overcome the defects of the gas-phase process (Koelbel and Ralek, 1980; Satterfield and Stenger, 1985). However, the diffusion of synthesis gas in the micropores of the catalysts was so slow in the slurry phase that the overall reaction rate was lower than that in the gas-phase reaction (Stern and Bell, 1983; Fujimoto, 1987).

It has been known that a supercritical fluid has a unique characteristic in its molecular diffusion and its solubility parameter (Debenedetti and Reid, 1986). We have studied the reaction performances of the supercritical F-T synthesis reaction from the viewpoint of the extraction capability of various solvents (Yokota et al., 1991).

In the present work, one of the main goals was to determine how the pore size of the catalyst affects the transfer of reactants and products in the supercritical-phase F-T synthesis reaction. In addition to the study of the reaction performance of the catalysts with different micropore size, the effect of the contact time of the reactant with the catalyst was also investigated.

Experimental

Catalyst preparation

Alumina-supported ruthenium catalysts were prepared by impregnating γ-alumina with ruthenium chloride from its aqueous solution (Fujimoto et al., 1983). The alumina supports with different pore size were prepared from aluminun nitrate and ammonia with the pH swing method (Ono et al., 1982). After precipitation with suitable times of pH swing, the resulting materials were calcined at 600°C for 2 h and were impregnated as mentioned above. Composition of the catalysts was *Ru*:2 and Al_2O_3:98 by weight. The catalyst precursors were dried overnight at 120°C in an air oven, and were then calcined at 450°C for 2 h to form a supported metal oxide and to make the ruthenium oxide particles grow on the surface (Fujimoto

Correspondence concerning this article should be addressed to K. Fujimoto.

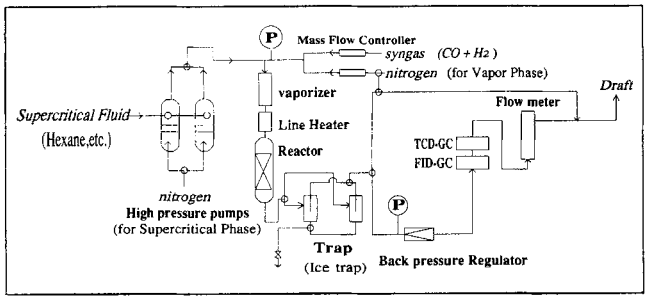

Figure 1. Reaction apparatus flow sheet.

and Kajioka, 1987). The catalysts were reduced in a hydrogen flow at 150°C, and 300°C for 1 h, respectively, and at 400°C for 2 h in series and then passivated; they were reduced again at 400°C for 2 h *in situ* before catalytic reaction. The series of *Ru* on pH swing Al_2O_3 is noted by the frequency of the pH swing.

Apparatuses for reaction and analysis

The reaction apparatus of the supercritical-phase reaction was similar to that of a conventional, pressurized, fixed-bed flow reactor system. The only difference was that a vaporizer and an ice-cooled high-pressure tap were set upstream and downstream of the reactor, respectively, as shown in Figure 1. N-hexane (C_6H_{14}), whose critical temperature and critical pressure are 233.7°C and 29.7 bar, respectively, was chosen as the supercritical solvent. The standard reaction conditions were $T = 240$°C, $P(\text{total}) = 45$ bar, $P(CO + H_2) = 10$ bar, $P(\text{balance gas}) = 35$ bar, $CO/H_2 = 1/2$, $W/F(CO + H_2) = 10$ g of catalyst h·mol^{-1}. Argon was used as internal standard with the concentration of 3% in the feed gas.

Reaction temperature was defined with the highest temperature of the catalyst bed, measured by a thermocouple which was placed along the center of the catalyst bed. Temperature profiles of the catalyst bed distributed within 1-2°C in the supercritical phase reaction.

Gaseous compounds were analyzed on-line by gas chromatographs. CO, CH_4 and CO_2 were analyzed by using an activated charcoal column with a thermal conductivity detector (TCD). Light hydrocarbons (C_1-C_6) were analyzed by a Porapak-Q column with a flame ionization detector (FID). Hydrocarbons dissolved in the solvent were analyzed with Silicone SE-30 and Dexil-300 GC columns with flame ionization detectors. Capillary columns (OV-1 bonded and OV-1701 bonded) were employed for the precise analysis of the products. Each reaction was conducted for 6 h. Extracted products were determined by extracting the remaining product with n-hexane at 250° for 1 h after reaction. The chain-growth probability (α value) of the product was defined by the Anderson-Schulz-Flory plot of the products, in which the carbon number extended from C_3 to C_{25} (Madon, 1979).

The dispersion of ruthenium metal was determined by means of hydrogen chemisorption. Chemisorption was measured at room temperature by using a flow-through cell connected to a glass vacuum system. Catalyst samples were first activated in flowing hydrogen *in situ* at 150°C for 1 h and at 450°C for 2 h, then evacuated at 450°C for 1 h. The metal dispersion was calculated assuming one hydrogen atom which was chemisorbed by one surface ruthenium atom. The particle size of ruthenium metal was calculated from the equation $D = 11/(H/Ru)$, where D is the diameter in angstroms and H/Ru is the ratio of the number of hydrogen atoms adsorbed divided by the number of *Ru* atoms in the catalysts (Anderson, 1975).

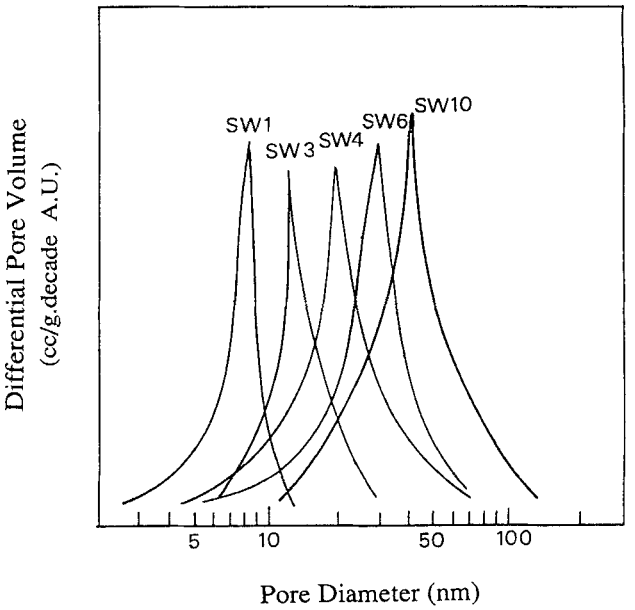

Figure 2. Pore distribution of various pH/swing catalysts.

The measurement of the pore distribution of the catalysts was conducted with a mercury porosimeter (Shimadzu 9200). X-ray diffraction (XRD) measurements were conducted with a Rigaku Rotaflex instrument using CuKα irradiation (40 kV, 100 mA).

Results and Discussion

Physical structures of Ru/Al_2O_3 catalysts

The pore-size distributions of pH-swing catalysts are shown in Figure 2. When the swing times increased from 1 to 10, the mean pore size of the catalyst increased from 8.5 nm to 33.5 nm and the specific surface area of the catalyst measured by BET method was reduced from 227 m^2/g to 139 m^2/g as well (Table 1).

Alumina is a kind of amphoteric oxide and it can precipitate in the form of pseudo-boehmite [AlO(OH)] when the pH is

Table 1. Physical Characterization of *Ru* Catalysts

Catalyst	SW1	SW3	SW4	SW6	SW10
Mean Pore Size (nm)	8.5	11.4	20.0	27.0	33.5
Pore Volume (cm^3/g)	0.67	0.86	1.07	1.20	1.34
Specific Surface Area (m^2/g)	227	210	184	164	139
Metal Size by H_2 Adsorption (Å)	37	41	53	79	100

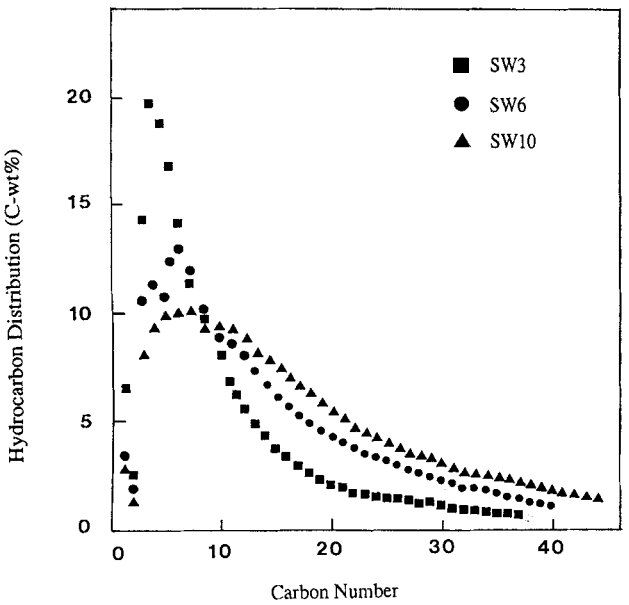

Figure 3. Hydrocarbon distribution of the products on supported ruthenium catalysts.

2 wt. % *Ru* on pH-swing aluminas, 240°C, 4.5 MPa (syngas 1.0 MPa, n-C_6 3.5 MPa), $CO/H_2 = 1/2$. W/F(syngas) = 10 g cat·h/mol.

kept between 8 and 10. As the amorphous aluminum hydroxide precipitate is also formed in this pH area, the resulting gelatin was the mixture of pseudo-boehmite and hydroxide particles with different sizes. Changing the pH value to the acidic side (pH = 2 or 2.5) would make aluminum hydroxide dissolve and only pseudo-boehmite was left. Aluminum salts of both acid and alkali were admixed alternately in the gelation process accompanied by a swinged pH value between 2 and 10. The aggregation of pseudo-boehmite particles only and the uniform growth of the pseudo-boehmite crystal were available by this way. Porous alumina could be obtained by the dehydration

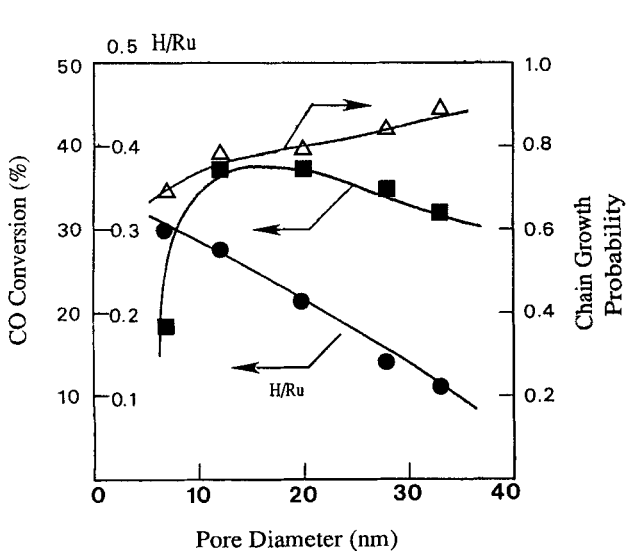

Figure 4. Relationship between mean pore size and *Ru* metal dispersion, the maximum CO conversion or the chain-growth probability.

The same reaction conditions as in Figure 3.

of pseudo-boehmite. When the pH values, swinging frequency and the reaction time under a specific pH value were changed, various kinds of alumina with different pore sizes can be prepared.

It is shown in Table 1 that the mean metal particle size increased from 3.7 nm to 10 nm as the specific surface area decreased. We reported that ruthenium chloride was converted to ruthenium oxide during air calcination and it can move easily on the carrier and aggregate into larger particles, as expected due to its high sublimation characteristics (Fujimoto et al., 1985).

It should be noted that XRD and chemisorption method were employed to investigate the possible change through reaction for used catalysts. No obvious changes occurred on them except tiny wax stayed inside. It has been found that alumina-supported *Ru* particles larger than 3 nm were stable and no agglomeration or loss of ruthenium was observed (Abrevaya et al., 1990).

The reaction behavior of the Ru catalysts with different pore size

Carbon Chain Growth. In Figure 3 are shown the carbon number distributions of the products on the SW3, SW6, and SW10 catalysts whose mean pore sizes are 11.4, 27.0 and 33.5 nm, respectively. The activities and selectivities of the catalysts are markedly different from one another, depending on the pore structure, even if they are loaded with the same amount of ruthenium. It is found that the product distribution of the SW10 catalyst was wider and the proportion of the heavy hydrocarbon was high. On the other hand, the catalyst having a small pore size, such as the SW3 catalyst, tended to produce relatively lighter hydrocarbons.

Figure 4 shows the CO conversion, the dispersion of ruthenium from hydrogen adsorption, and the chain-growth probability as a function of catalyst pore diameter. It is clear from the data in Figure 4 that the chain-growth probability of the *Ru* catalysts increased while the *Ru* dispersion decreased with the increase in the pore diameter. The high ability of carbon-carbon bond formation of the large pore catalyst should be attributed to its large *Ru* particles. It has been already pointed out that the propagation of the carbon-carbon chain occurred more easily because the ruthenium particle size became larger on the catalysts with lower specific surface area (Nijs and Jacobs, 1980; Fujimoto et al., 1985). The increased chain-growth probability occurring on the catalyst of larger pore size might be attributed to the larger ruthenium particle size as well as the larger and uniform pore size (Table 1). The dispersion of the supported ruthenium metal and the pore size of the catalyst show their close relationship with the propagation of the carbon chain even in the case of supercritical phase reaction. This may be regarded as evidence supporting the suggestion that the supercritical fluid (n-hexane) should show little effect on the reaction mechanism itself.

Table 2 shows the reaction behaviors of the SW3, SW6, and SW10 catalysts. The activity of the SW10 catalyst was slightly lower than that of the SW3 or SW6 catalyst. The principal factor which controlled the catalytic activity is discussed in the following session.

Mass transfer in the catalyst pores. The ratio of the hydrocarbon product which was extracted from the catalyst bed

Table 2. Reaction Behavior in the Supercritical Phase of the Catalysts with Different Pore Size

Catalyst	SW3	SW6	SW10
CO Conversion (%)	37	35	32
Total Products (a) (C mmol/g cat·h)	18.4	17.1	15.7
Extracted Products (b) (C mmol/g cat·h)	0.66	0.46	0.32
Residual Ratio (%) (b)/(a)	3.6	2.7	2.0
Methane Selectivity (%)	6.6	3.1	2.3
Avg. Olefin Content (%)	41.7	49.3	52.6

after each reaction to the total amount of the hydrocarbon product (residual ratio) is an important index for the Fischer-Tropsch synthesis reaction. We reported that the residual ratio in the supercritical-phase reaction was remarkably lower than that in the gas-phase reaction and was similar to that in the liquid-phase reaction (Yokota and Fujimoto, 1989). It is clear from the data in Table 2 that the residual ratio of the products decreased with increased catalyst pore size, in spite of more waxy products formed on the large-pore catalyst because of its high chain growth probability. This fact reflects that the *in situ* extraction of the product by the supercritical fluid occurred more effectively for the catalyst with larger pores. The fine balance between the rates of the product desorption from the catalyst surface and its transfer from the catalyst pores is the characteristic feature for the effective overall transfer of the product in the supercritical phase reaction (Yokota and Fujimoto, 1991). It is clear from the data that the transfer of the desorbed product inside the pores was more rapid and more efficient for the large pore catalyst, as expected, even if its higher chain growth probability made product more waxy.

The discussion above might be also supported by the result of the olefin content and the methane selectivity in the products. The average olefin content of the product on SW10 catalyst was 53% while that on SW3 catalyst was 42%. In the F-T synthesis reaction, 1-olefins are generally produced as the primary products and are successively hydrogenated to paraffins (Storch et al., 1951; Henrici-Olive and Olive, 1984; Anderson, 1984). When the pore size is larger, the transportation of the primary product is more effective and relevantly the degree of secondary hydrogenation of olefins is lower. The methane selectivity shown in Table 2 is the lowest for the largest pore catalyst. Methane can be formed directly from syngas as primary product, also it can be formed by hydrocracking of primarily formed 1-olefins on the ruthenium catalyst. In fact the change of chain growth probability hardly shows effect on methane selectivity. So the decrease of methane formation for larger pore catalyst might be mainly attributed to the quick diffusion of 1-olefins inside pores and the lower possibility for secondary hydrocracking. Due to the highly effective diffusion of the primary product (mainly 1-olefin) from the inside of the catalyst, especially in the case of the catalyst with the largest pores, the probability of the secondary reaction of 1-olefin was lower, thus the degree of the secondary hydrogenation and the hydrocracking was lower. As a result a lower methane selectivity can be achieved for the large pore-size catalyst in the supercritical phase reaction.

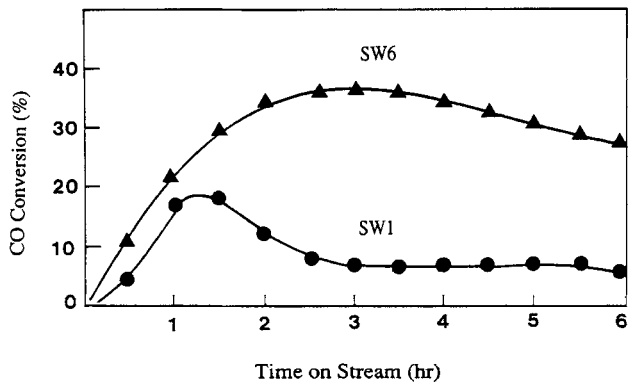

Figure 5. Pore size effect on the activity change of *Ru* catalysts.

The same reaction conditions as in Figure 3.

Influence of pore size on the activity of Ru catalysts

Influence of pore size on the durability of Ru/Al_2O_3 catalyst. The change of catalytic activity with reaction time is shown in Figure 5. SW1 and SW6 represent *Ru* catalysts with smaller and larger pore sizes, respectively (see Table 3). It could be found that the small-pore catalyst exhibited low catalytic activity, reached the maximum conversion soon, and then decreased to a lower level. On the other hand, the activity of the catalyst of larger pore size was high and changed gradually. The reason for this phenomenon is not clear yet.

Catalytic activity as a function of pore size. The apparent rate constant increased, as shown in Figure 4, with increasing pore diameter to reach a maximum at around 15 nm and then gradually decreased with further increase in the pore size. This phenomenon is explained in terms of two reasons. One is that the catalyst with a small pore size owns a larger specific surface area and the ruthenium metal dispersion is highest. It was reported that the turnover frequency (TOF) of this reaction on alumina-supported ruthenium catalysts under atmospheric conditions decreased with an increase in the dispersion (King, 1978; Kellner and Bell, 1981). We also reported that under pressurized conditions the specific activity of supported ruthenium catalysts increased as the dispersion decreased, irrespective of the carrier materials (Fujimoto et al., 1985). In fact, as is clear from the data in Figure 4, the ruthenium dispersion determined by hydrogen chemisorption decreases with increasing pore size. Another reason is that the modal pore size of the catalyst was so small that the diffusion of syngas was remarkably retarded. In fact, not only the concentration of the reactants inside the pores but also the effectiveness factor of the catalyst was decreased when the mean pore diameter of the catalyst was small, especially in the liquid-phase reaction (Fujimoto, 1987) and also in the supercritical phase. This concept will be simulated in the latter session.

Temperature characteristics of the catalysts with various pore size. Figure 6 shows the Arrhenius plots of the CO conversion rate of three kinds of ruthenium catalysts with the same particle size (2 mm), in which the mean pore size varies

Table 3. Simulation Results for pH-Swing Catalysts

Catalyst	SW-1	SW-3	SW-4	SW-6	SW-10
Pore Size (Å)	84	120	200	270	335
H/*Ru* Ratio	0.30	0.27	0.21	0.14	0.11
k (s^{-1})	8.1	7.3	5.7	3.8	3.0
R (mm)	0.5	0.5	0.5	0.5	0.5
D_{H2} (10^{-9} m^2/s)	2.13	4.91	11.4	16.7	21.8
D_{CO} (10^{-9} m^2/s)	1.54	3.55	8.26	12.0	15.7
Thiele Modulus ϕ	10.3	6.4	3.7	2.5	1.95
Catalyst Effective Factor η	0.094	0.148	0.245	0.345	0.424
$k\,\eta$	0.76	1.08	1.39	1.31	1.27

from 8.5 nm to 30 nm. In the case of a small mean pore size (8.5 nm, SW1), the apparent activation energy was only 17 kcal/mol, which was remarkably lower than those of the catalysts with mean pore sizes larger than 10 nm.

As proven elsewhere (Madon and Boudart, 1982), when the diffusion of reactant limits the overall reaction rate, the apparent activation energy of the reaction is indicated by the arithmetical mean of the two apparent activation energies in the diffusion-controlled regime and in the reaction-controlled regime. As we have seen in Figure 6, the apparent activation energy decreased with a decrease in the pore size of the catalyst. The lower catalyst activity and the lower apparent activation energy for the catalyst with smaller pores should be attributed to the low rate of synthesis gas diffusion in the catalyst pores compared to the rate of the surface reaction, resulting from the high ratio of the reaction rate to the mass-transfer rate when the surface area to pore volume ratio is high (Table 1).

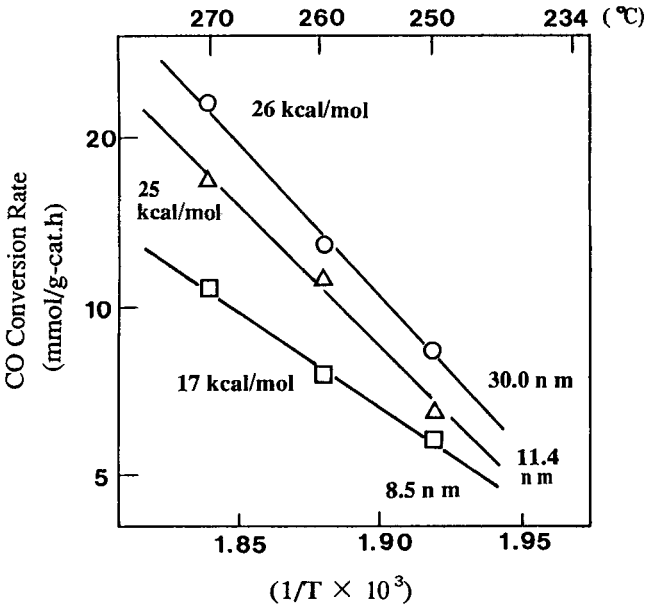

Figure 6. Arrhenius plots of CO conversion rate of *Ru* catalysts with various pore size.

Catalyst particle size: 2 mm, 2 wt. % *Ru* on pH-swing alumina, SW-1 (8.5 nm), SW-3 (11.4 nm) and SW-9 (30.0 nm). The number in parentheses is the catalyst pore size in nanometer. Pressure: 4.5 MPa (syngas 1.0 MPa, *n*-hexane 3.5 MPa), $CO/H_2 = 1/2$, W/F(syngas) = 2 g cat·h/mol.

The high reaction to mass-transfer ratio should be more eminent in the small pore catalyst and at high reaction temperature.

In our previous reports (Yokota et al., 1990; Yokota and Fujimoto, 1991), the influence of catalyst particle size on the rate constant was inspected in the gas-phase and supercritical phase F-T reaction. It was found that the apparent activation energy for gas-phase reaction was not influenced by catalyst particle size but in the supercritical reaction, when the catalyst particle size increased, the reaction rate and the apparent activation energy decreased. Because mass-transfer rate in supercritical fluid is not as quick as that in gas, the criteria proposed by Madon and Boudart (Madon and Boudart, 1982) for intrinsic rate measurement of heterogeneous catalytic reactions could not be satisfied here and the measured catalytic activity was dependent on influence of transportation velocity.

Simulation of the diffusion of reactants and the effectiveness factor of the catalyst in the supercritical-phase reaction

In this section, a theoretic explanation is attempted for the experimental results above.

Mathematical model. Under the supercritical-phase reaction conditions, the influence of laminar diffusion could be neglected. Suppose the catalyst pellet is a sphere with radius R and consider the mass equilibrium inside a shell of the catalyst pellet,

$$D_{H2}\left(\frac{d^2C_{H2}}{dr^2}+\frac{2dC_{H2}}{rdr}\right)-V_{H2}=0 \tag{1}$$

$$D_{CO}\left(\frac{d^2C_{CO}}{dr^2}+\frac{2dC_{CO}}{rdr}\right)-V_{CO}=0 \tag{2}$$

where r is the radius of the shell; D_{H2} or D_{CO}, whose calculation is discussed in the next section, is the effective diffusion coefficient for hydrogen or carbon monoxide in supercritical phase; V_{H2} or V_{CO} is the reaction rate per unit volume for H_2 or CO; and C_{H2} and C_{CO} are the concentrations of reactants.

The boundary conditions are:

$$r=R \quad C_{H2}=C_{H2,0} \quad C_{CO}=C_{CO,0}$$

$$r=0 \quad \frac{dC_{H2}}{dr}=\frac{dC_{CO}}{dr}=0$$

Generally-speaking, a power rate law has been represented for F-T reaction kinetics, and the rate can be shown by the following equation:

$$V = kP_{H2}{}^{x}P_{CO}{}^{y}$$

where k is the rate constant and x and y are the exponential dependencies on H_2 and CO pressures, respectively. It is often recognized that the reaction orders for the Fischer-Tropsch synthesis reaction on ruthenium catalysts with respect to hydrogen and carbon monoxide is one and zero, respectively (Vannice, 1976; Karn et al., 1965; Vannice, 1975; Dry, 1981; Post et al., 1989).

$$V_{H2} = k\,C_{H2} = 2\,V_{CO} \tag{3}$$

where k is the reaction constant. From Eqs. 1 and 3, the distribution of the hydrogen concentration can be expressed as:

$$\frac{C_{H2}}{C_{H2,0}} = \frac{\sinh(3\phi\, r/R)}{(r/R)\sinh(3\phi)} \tag{4}$$

where the Thiele modulus

$$\phi = \frac{R}{3}\left(\frac{k}{D_{H2}}\right)^{1/2} \tag{5}$$

From Eqs. 1-3, the relationship between the hydrogen and carbon monoxide concentrations can be derived:

$$C_{CO} = \frac{D_{H2}}{2D_{CO}}\,(C_{H2} - C_{H2,0}) + C_{CO,0} \tag{6}$$

So the catalyst effectiveness factor η can be derived as:

$$\eta = \frac{1}{\phi}\left(\frac{1}{\tanh(3\phi)} - \frac{1}{3\phi}\right) \tag{7}$$

Thus the apparent rate constant for each catalyst can be expressed as:

$$k\eta\frac{4\pi C_{H2,0}R^3}{3}$$

Calculation of the diffusion coefficient. Although the precise calculation of the diffusion coefficient for molecules in a supercritical medium is very difficult (Debenedetti and Reid, 1986), it is practical to apply the Stokes-Einstein method in hydrodynamics as well as the experimental verification.

$$D = \frac{K_B T}{6\pi a f} \tag{8}$$

where D is the diffusion coefficient of a Brownian sphere of radius a in a continuum with viscosity f and temperature T, when no slip exists between the particle and the continuum. K_B is the Boltzmann constant. Considering the reaction conditions, the viscosity of n-hexane at 240°C and 35 atm is calculated from a handbook (Japan Chemical Society, 1984) to be 0.0706 cp (7.06×10^{-5} kg/m·s), and the radius of the hydrogen molecule or carbon monoxide molecule (the long axis of diatom molecule) is 1.57Å or 2.18Å, respectively. With these data, the molecular diffusion coefficient can be estimated to be 3.39×10^{-8} m²/s for hydrogen and 2.48×10^{-8} m²/s for carbon monoxide, respectively.

The molecular diffusion coefficient obtained above is suitable for diffusion occurring in a pure supercritical fluid. In order to calculate the effective diffusion coefficient *De* for the catalyst in the supercritical fluid, the shape of the catalyst pellets must be considered, that is,

$$De = \frac{\epsilon}{\tau}D \tag{9}$$

where ϵ is the void fraction and τ is the tortuosity factor of the catalyst pellet. As the tortuosity factor is difficult to get, it is approximately expressed as:

$$\tau = \frac{1}{\epsilon} \tag{10}$$

so,

$$De = \epsilon^2 D \tag{11}$$

For the standard catalyst (*Ru*/JRC-ALO-4) which was used mostly in our previous work, the void fraction measured by mercury porosimeter was 0.635; in this way, *De* is 13.7×10^{-9} m²/s for hydrogen and 9.90×10^{-9} m²/s for carbon monoxide.

The calculation above can also be demonstrated from experiment. If the gas-phase reaction is regarded as the ideal state for the diffusion of the reactants, it should show:

$$\frac{V_{SC}}{V_G} = \eta \tag{12}$$

where η is the catalyst effectiveness factor and V_{SC} and V_G are the reaction rates in the supercritical phase or gas phase. It should be noted that the reaction rates here, which are regarded as intrinsic rates (without diffusion limitation), should be near the observed results with well crushed catalyst particles having an average particle size of 0.2 mm. By utilizing Eqs. 7 and 5; the effective diffusion coefficients can be deduced in reverse order. From published experimental results with the gas-phase and supercritical-phase F-T reactions on a ruthenium catalyst (*Ru*/JRC-ALO-4) (Yokota et al., 1990), the experimental effective diffusion coefficient for hydrogen can be calculated to be 9.7×10^{-9} m²/s and that for carbon monoxide is 7.0×10^{-9} m²/s, which are nearly the same as the theoretical values shown previously, that is, 13.7×10^{-9} m²/s for hydrogen and 9.90×10^{-9} m²/s for carbon monoxide.

Simulation results and their accordance with the experiments. The effect of catalyst particle size on the concentration distributions inside the catalyst particles is shown in Figure 7. The *Ru*/Al_2O_3 catalyst used here is a standard catalyst (*Ru*/JRC-ALO-4) which was mostly used in our previous report. Experimentally, when the particle size was 2 mm, the catalyst activity in the supercritical phase was about one-third that of

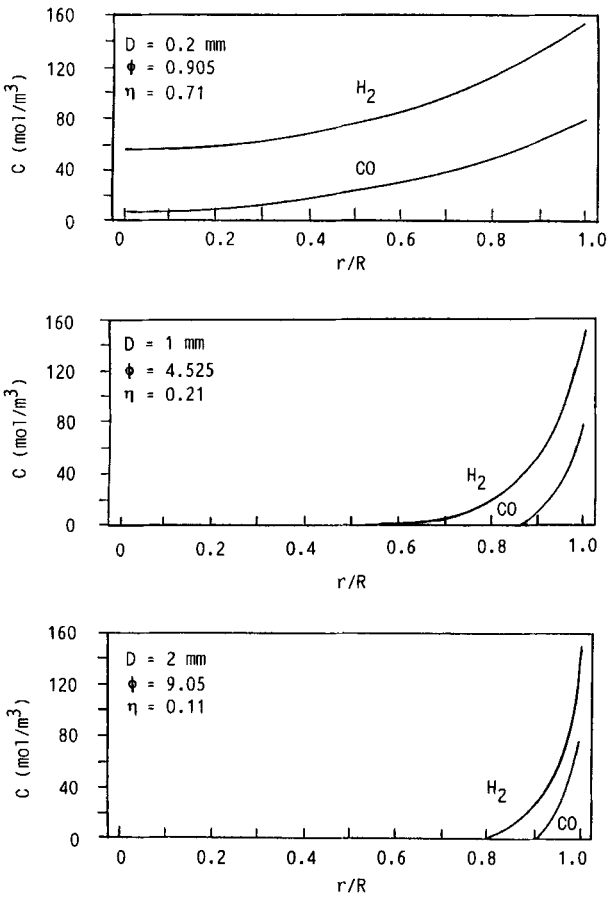

Figure 7. Simulation of the effect of catalyst particle size on the reactant concentration profiles inside the particles. 2 wt. % *Ru* on Al_2O_3 (JRC-ALO-4).

$CO/H_2 = 1/2$; pressure, 4.5 MPa (syngas 1.0 MPa, *n*-hexane 3.5 MPa); W/F(syngas) = 10 g cat·h/mol; D = diameter of catalyst particles; ϕ = Thiele modulus; η = effectiveness factor of catalyst.

the small size (0.2 mm) catalyst. Also, the apparent activation energy was 4 kcal/mol lower than that for the small size catalyst. The simulated results show the concentration profiles of reactants inside the catalyst particles. Significant profiles were formed inside the catalyst particles, especially for the larger particles. As a result, the catalyst effectiveness factor decreased from 0.71 to 0.11 as the diameter of the catalyst particle increased from 0.2 mm to 2 mm.

It is found that the effectiveness factor of the small pore catalyst is so low that the catalyst activity remains very low even though its reaction rate constant is the highest. It means that the inner surface of this kind of catalyst is hardly utilized. On the other hand, the effectiveness factor for the larger pore catalyst, for example the SW-10 catalyst, shows a higher value but its reaction rate constant is not as high because of the relatively lower specific surface area of *Ru* metal. As a result, the activity of the catalyst having the largest pore size is not the highest, and the activities of the catalysts with moderate pore size are the highest due to this compromise effect. This result is consistent with the experiment results, as shown in Figure 8.

Effect of pore size on the product diffusion. Figure 9 shows

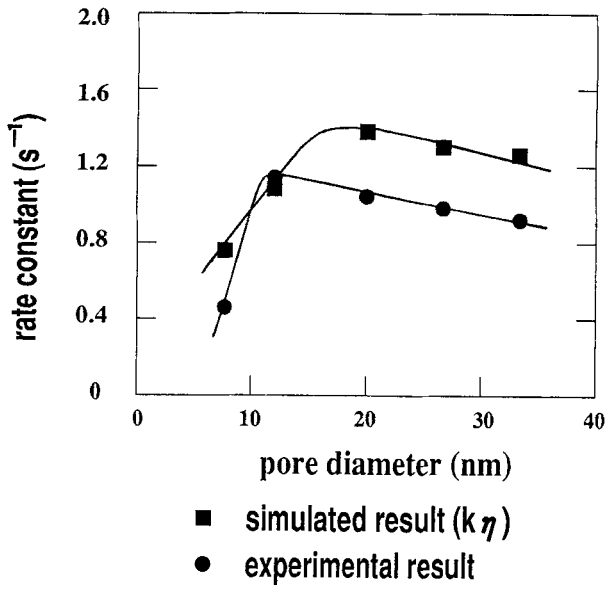

Figure 8. Comparation between experimental and simulation results for pH-swing catalysts.

The same reaction conditions as in Figure 3.

the olefin content in the product from catalysts with different pore sizes. Among the light C_2 to C_{10} hydrocarbons, there is little difference. The olefin content in the product was still as high as 40% for the C_{20} hydrocarbon in the case of the large pore (33.5 nm) catalyst even though the catalytic activity was still high, while the olefin content in the product from a smaller pore (11.4 nm) catalyst decreased remarkably with increasing carbon number of the product and reached to zero around C_{20}. For a specific catalyst, it is shown that olefin content of its light hydrocarbon was higher while the percentage of the paraffinic product increased as carbon number increased. Also, as an exception, the ratio of ethylene was very low.

The high olefin content of the product from the catalyst with the largest pore size is a reasonable phenomenon because a relatively more effective mass transfer occurred for the higher molecular weight product. As a result, the degree of secondary hydrogenation reaction was suppressed. It was reported that the dispersion of ruthenium metal showed little influence on the olefin-to-paraffin ratio in low carbon number products in

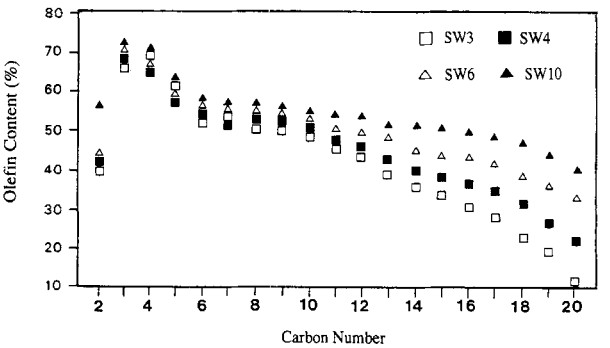

Figure 9. The effect of catalyst pore size on the olefin content of the product from a *Ru*-catalyzed reaction: the standard reaction conditions.

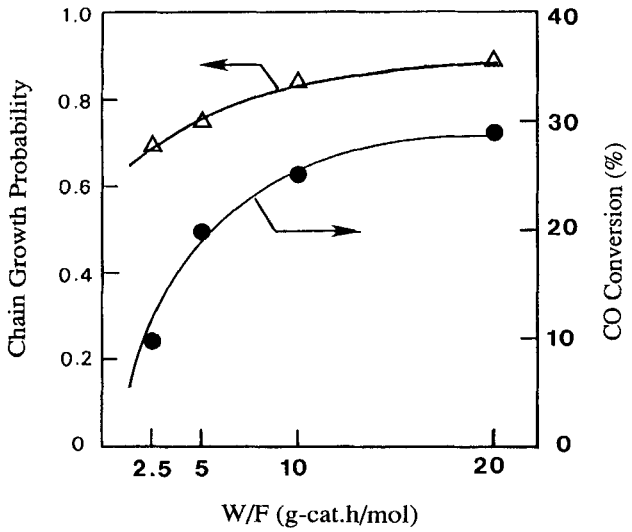

Figure 10. Relationship between contact time of the reactant gas and CO conversion and the chain-growth probability: *Ru*/SW6 catalyst, the standard reaction conditions except contact time.

the gas-phase F-T synthesis reaction (Kellner and Bell, 1982), so the differences in metal dispersion of the pH-swing catalysts here are presumed not to be important in determining the olefin content in the products from a supercritical-phase F-T reaction.

Recently, it was proposed that the higher solubility of larger olefins increased their reactor residence time and enhanced their chances of undergoing secondary reactions (Tau et al., 1990). Some pertinent research (Madon et al., 1991; Iglesia et al., 1991) showed that in gas-phase F-T reaction primary 1-olefin readsorption and surface chain initiation took place as

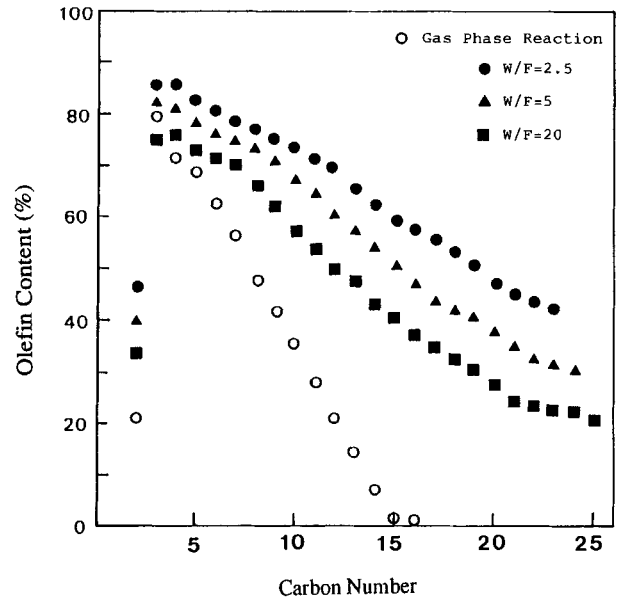

Figure 11. The influence of the contact time of the reactant gas on the olefin content in the products: *Ru*/SW6 catalyst, standard reaction conditions except contact time.

secondary reactions. Also readsorption of 1-olefins increased with molecular size because the rate of removal of olefins from liquid-filled catalyst pores is decreased due to intraparticle diffusion limitation. Our observations for the supercritical phase F-T reaction seems to be supported by their research. We believe that the readsorption of 1-olefins onto FT-active sites play a crucial role in the synthesis of high molecular weight hydrocarbons. Heavier 1-olefins remained longer within catalyst pores because of their decreased diffusivities and readsorbed onto *Ru* sites more easily to receive secondary hydrogenation to form paraffin. Paraffinic products do not undergo any further reaction and exit the pore unreacted. On the other hand, the pore-size effect on the product selectivity behaved by the way of changing the diffusivities of primary 1-olefins. Relatively more effective diffusion for the olefins within larger catalyst pores leads to high olefin content in the product of large core catalyst.

The olefin content for C_2 (ethylene) is obviously lower than those of other light hydrocarbons. Some reports showed that yields for C_2, in some cases including C_3, were low and fall below those predicted by the Schulz-Flory distribution (Kellner and Bell, 1981). In our results (also shown in Figure 3) these low values reflect the rapid rate of ethylene readsorption and chain initiation, including their incorporation into growing chains.

The influence of the contact time. In Figure 10 is displayed the effect of the contact time on CO conversion and the chain-growth probability. When the contact time changed from 2.5 to 5 g cat·h/mol, the CO conversion increased rapidly then increased slowly to about 30% as the contact time increased from 5 to 20 g cat·h/mol. While the contact time changed from 2.5 to 20 g cat·h/mol, the chain-growth probability increased from 0.70 to 0.91.

It is rational that a long contact time of synthesis gas is favorable for the propagation of carbon chains, because the primary products (1-olefins) might be re-adsorbed on the ruthenium sites and be subjected to secondary carbon chain propagation (Henrici-Olive and Olive, 1984; Madon and Iglesia, 1991).

Figure 11 shows that the olefin content of the product was affected by the contact time (W/F). When the contact time was increased, the olefin content decreased, but its level is much higher than that of the product from the gas-phase reaction. The low olefin content in the products from the gas-phase reaction, especially the higher molecular weight portion, can be attributed to their slow desorption from the catalyst surface and the resultant secondary hydrogenation.

In general, the rate of removal of 1-olefins from the catalyst bed is controlled by intraparticle diffusion (pore residence time) and contact time (bed residence time). In the gas-phase reaction, intraparticle diffusion dominates the removal rate of the larger reactive molecules and contact time has no effect on the pore residence time or on the readsorption of larger 1-olefins but controls the residence time of hydrocarbons outside liquid-filled pores. As a result, the effect of contact time on readsorption is most apparent for light olefins in the gas-phase F-T reaction. But in the supercritical phase F-T reaction, because of high diffusion and high density of the supercritical fluid and its quick in situ extraction for waxy product, the olefin content of both light and heavy hydrocarbons is controlled by the contact time.

Conclusions

Reaction engineering associated with the supercritical-phase Fischer-Tropsch synthesis reaction was studied in terms of the mass transfer of the reactants or products.

Tailor-made catalyst supports with a sharp pore diameter distribution could be prepared by the pH swing method. The catalyst pore size can control the catalytic activity as well as the distribution of the products because of the differences in the diffusion of both reactants and products.

In the supercritical-phase reaction using the larger-pore catalysts, waxy products could be effectively extracted *in situ* while the hydrogenation or the hydrocracking of olefins was effectively suppressed. Both the desorption and the diffusion of the product were so well balanced that the overall mass transfer of the products was most effective in the supercritical phase.

The ruthenium catalyst having a moderate pore size showed the highest activity while the catalyst with the largest pore size exhibited the highest chain-growth probability. The effects of metal particle size and pore size on the catalytic activity were reasonably simulated based on the diffusive behavior of the synthesis gas, in terms of the calculated effectiveness factor and the apparent Arrhenius activation energies of *Ru* catalysts with different pore sizes or particle sizes.

Acknowledgment

The technical help from Tokyo Gas Co. Ltd. and Chiyoda Chemical Engineering & Construction Co. Ltd. is gratefully acknowledged. This work was financially supported by the Grant-in-Aid of Ministry of Education, Science and Culture, Japan.

Notation

a = radius of Brownian sphere, m
C = concentration, mol/m^3, or carbon number
D = diffusion coefficient, m^2/s
De = effective diffusion coefficient, m^2/s
f = viscosity, kg/m·s
F = flow rate, mol/h
k = reaction rate constant, s^{-1}
K_B = Boltzmann's constant, J/K
P = pressure, Pa
r = radial position within a particle
R = radius of particle
T = temperature, K
V = reaction rate, mol·m^{-3}·s^{-1}
W = weight, g
x = exponential dependency
y = exponential dependency

Greek letters

α = chain growth probability
ϵ = void fraction of catalyst
ϕ = Thiele modulus
η = effectiveness factor of catalyst
τ = tortuosity factor of catalyst

Subscripts

CO = carbon monoxide
G = gas phase
H_2 = hydrogen
i = carbon number
0 = state outside a particle
SC = supercritical phase

Literature Cited

Abrevaya, H., M. J. Cohn, W. M. Targos, and H. J. Robota, "Structure Sensitive Reactions over Supported Ruthenium Catalysts During Fischer-Tropsch Synthesis," *Catal. Lett.*, **7**, 183 (1990).

Anderson, R. B., *The Fischer-Tropsch Synthesis*, Academic Press, Orlando, FL (1984).

Anderson, J. R., *Structure of Metallic Catalysts*, Academic Press, London (1975).

Debenedetti, P. G., and R. C. Reid, "Diffusion and Mass Transfer in Supercritical Fluids," *AIChE J.*, **32**, 2034 (1986).

Dry, M. E., "The Fischer-Tropsch Synthesis," *Catalysis, Science and Technology*, Vol. 1, J. R. Anderson and M. Boudart, eds., Springer-Verlag, Berlin (1981).

Fujimoto, K., "Reaction Engineering for Slurry Phase Fischer-Tropsch Synthesis," *Reports of the Special Project on Energy under Grant in Aid of Scientific Research of the Ministry of Education, Science and Culture*, p. 199 (1987).

Fujimoto, K., and M. Kajioka, "Hydrogenation of Carbon Monoxide over Solid Catalysts Dispersed in the Liquid Medium. I. Slurry-Phase Fischer-Tropsch Synthesis with Supported Ruthenium Catalysts," *Bull. Chem. Soc. Jpn.*, **60**, 2237 (1987).

Fujimoto, K., H. Saima, and H. Tominaga, "Fischer-Tropsch Synthesis with Supported Cobalt Catalysts," *J. Japan Petrol. Inst.*, **26**(4), 258 (1983).

Fujimoto, K., T. Nobusawa, T. Fukushima, and H. Tominaga, "Activity and Selectivity Regulation of Synthesis Gas Reaction over Supported Ruthenium Catalysts," *Bull. Chem. Soc. Jpn.*, **58**, 3164 (1985).

Henrici-Olive, G., and S. Olive, *The Chemistry of the Catalyzed Hydrogenation of Carbon Monoxide*, Chap. 9, Springer-Verlag, Berlin (1984).

Iglesia, E., S. C. Reyes, and R. J. Madon, "Transport-Enhanced α-Olefin Readsorption Pathways in Ru-Catalyzed Hydrocarbon Synthesis," *J. Catal.*, **129**, 238 (1991).

Japan Chemical Society, *Chemical Handbook (Fundamental) Part 2*, Maruzen, Tokyo (1984).

Karn, F. S., J. F. Schultz, and R. B. Anderson, "Hydrogenation of Carbon Monoxide and Carbon Dioxide on Supported Ruthenium Catalysts at Moderate Pressures," *Ind. Eng. Chem. Prod. Res. Dev.*, **4**, 265 (1965).

Kellner, C. S., and A. T. Bell, "Synthesis of Oxygenated Products from Carbon Monoxide and Hydrogen over Silica- and Alumina-Supported Ruthenium Catalysts," *J. Catal.*, **71**, 288 (1981).

Kellner, C. S., and A. T. Bell, "Effects of Dispersion on the Activity and Selectivity of Alumina-Supported Ruthenium Catalysts for Carbon Monoxide Hydrogenation," *J. Catal.*, **72**, 251 (1982).

King, D. L., "A Fischer-Tropsch Study of Supported Ruthenium Catalysts," *J. Catal.*, **51**, 386 (1978).

Koelbel, H., and M. Ralek, "The Fischer-Tropsch Synthesis in the Liquid Phase," *Catal. Rev. Sci. Eng.*, **21**, 225 (1980).

Madon, R. J., "On the Growth of Hydrocarbon Chains in the Fischer-Tropsch Synthesis," *J. Catal.*, **57**, 183 (1979).

Madon, R. J., and M. Boudart, "Experimental Criterion for the Absence of Artifacts in the Measurement of Rates of Heterogeneous Catalytic Reactions," *Ind. Eng. Chem. Fundam.*, **21**, 438 (1982).

Madon, R. J., S. C. Reyes, and E. Iglesia, "Primary and Secondary Reaction Pathways in Ruthenium-Catalyzed Hydrocarbon Synthesis," *J. Phys. Chem.*, **95**, 7795 (1991).

Nijs, H. H., and P. A. Jacobs, "Metal Particle Size Distributions and Fischer-Tropsch Selectivity. An Extended Schulz-Flory Model," *J. Catal.*, **65**, 328 (1980).

Ono, T., Y. Ohguchi, and O. Togari, "Control of the Pore Structure of Porous Alumina," Preprint of Int. Symp. on Catalyst Preparation, Belgium, G3 (1982).

Post, M. F. M., A. C. van't Hoog, J. K. Minderhoud, and S. T. Sie, "Diffusion Limitations in Fischer-Tropsch Catalysts," *AIChE J.*, **35**(7), 1107 (1989).

Satterfield, C. N., and H. G. Stenger, Jr., "Effect of Liquid Composition on the Slurry Fischer-Tropsch Synthesis: 1. Rate of Reaction; 2. Product Selectivity," *Ind. Eng. Chem. Process Des. Dev.*, **24**, 407 (1985).

Stern, D., A. T. Bell, and H. Heinemann, "Effects of Mass Transfer on the Performance of Slurry Reactors used for Fischer-Tropsch Synthesis," *Chem. Eng. Sci.*, **38**(4), 597 (1983).

Stern, D., A. T. Bell, and H. Heinemann, "Analysis of the Design of Bubble-Column Reactors for Fischer-Tropsch Synthesis," *Ind. Eng. Chem. Process Des. Dev.*, **24**, 1213 (1985).
Storch, H. H., N. Golumbic, and R. B. Anderson, *The Fischer-Tropsch and Related Synthesis*, John Wiley, New York, p. 309 (1951).
Tau, L. M., H. A. Dabbagh, and B. H. Davis, "Fischer-Tropsch Synthesis:^{14}C Tracer Study of Alkene Incorporation," *Energy & Fuels*, **4**, 94 (1990).
Vannice, M. A., "The Catalytic Synthesis of Hydrocarbons from H_2/CO Mixtures over the Group VIII Metals," *J. Catal.*, **37**, 449 (1975).
Vannice, M. A., "Catalytic Synthesis of Hydrocarbons from Carbon Monoxide and Hydrogen," *Catal. Rev. Sci. Eng.*, **14**, 153 (1976).
Yokota, K., and K. Fujimoto, "Supercritical Phase Fischer-Tropsch Synthesis Reaction," *Fuel*, **68**(2), 255 (1989).
Yokota, K., and K. Fujimoto, "Supercritical Phase Fischer-Tropsch Synthesis Reaction: 2. The Effective Diffusion of Reactant and Products in the Supercritical-Phase Reaction," *Ind. Eng. Chem. Res.*, **30**(1), 95 (1991).
Yokota, K., Y. Hanakata, and K. Fujimoto, "Supercritical Phase Fischer-Tropsch Synthesis," *Chem. Eng. Sci.*, **45**(8), 2743 (1990).
Yokota, K., Y. Hanakata, and K. Fujimoto, "Supercritical Phase Fischer-Tropsch Synthesis Reaction: 3. Extraction Capability of Supercritical Fluids," *Fuel*, **70**, 989 (1991).

Manuscript received Feb. 7, 1992, and revision received May 18, 1992.